ACS APPLIED MATERIALS & INTERFACES

Research Article

www.acsami.org

Metal Cation Cross-Linked Nanocellulose Hydrogels as Tissue Engineering Substrates

Nicole E. Zander,*[,†] Hong Dong,[†,‡] Joshua Steele,[†] and John T. Grant[§]

[†]United States Army Research Laboratory, Weapons and Materials Research Directorate, Aberdeen Proving Ground, Maryland 21005, United States

[‡]Bowhead Science and Technology LLC, Belcamp, Maryland 21017, United States

[§]Research Institute, University of Dayton, 300 College Park, Dayton, Ohio 45324, United States

ABSTRACT: The use of cellulose materials for biomedical applications is attractive due to their low cost, biocompatibility, and biodegradability. Specific processing of cellulose to yield nanofibrils further improves mechanical properties and suitability as a tissue engineering substrate due to the similarity to the fibrous structure, porosity, and size-scale of the native extracellular matrix. In order to generate the substrate, nanocellulose hydrogels were fabricated from carboxylated cellulose nanofibrils via hydrogelation using metal salts. Hydrogels cross-linked with Ca^{2+} and Fe^{3+} were investigated as tissue culture substrates for C3H10T1/2 fibroblast cells. Control substrates as well as those with physically adsorbed and covalently attached fibronectin protein were evaluated with X-ray photoelectron spectroscopy (XPS), Fourier transform infrared (FTIR), and enzyme linked immunosorbent assay (ELISA). Significantly more cells were attached to surfaces modified with protein, with the highest number of cells adhered to the calcium cross-linked hydrogels with covalently attached protein.

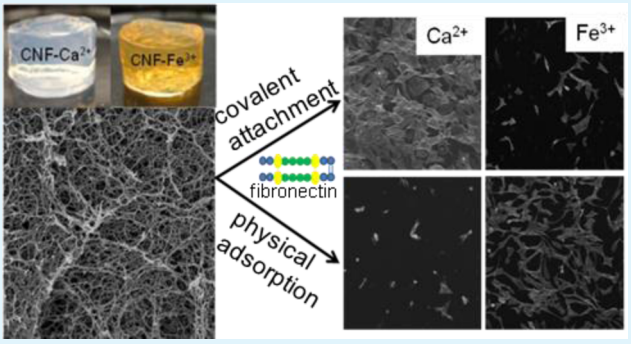

KEYWORDS: *nanocellulose, tissue engineering, fibroblasts, fibronectin, XPS, FTIR*

INTRODUCTION

The primary role of a tissue engineering scaffold is to provide a three-dimensional foundation to direct cellular attachment, proliferation, and differentiation, promoting tissue formation.[1,2] The choice of acceptable materials is restrictive because the materials must meet several basic characteristics. First, they must be biocompatible to the host tissue and not evoke an immune response. In addition, they should be sufficiently porous in order to support vascularization, nontoxic, and biodegradable.[3] Further, proper mechanical properties, matching those of the tissue they are replacing, as well as high surface area and a modifiable surface are important.[4−7]

Substrates with nanometer-sized features such as nanofibers or nanofibrils are highly desirable due to their similar size-scale and physical morphology as the natural collagen fibrils in the extracellular matrix (ECM).[8] The large surface-area-to-volume, due to the small diameters, is favorable for cell attachment and surface modification to improve cell adhesion. In addition, these materials generally have high porosity, which is critical for cellular infiltration, nutrient diffusion, and waste removal.[9,10] Nanofibers are generally formed from drawing, template synthesis, phase-separation, molecular self-assembly, or electrospinning.[11]

Cellulose from plant sources represents a virtually unlimited source of renewable material for biomedical applications and has long been used in sutures and wound dressings.[12−14] Although cellulose is biocompatible, biodegradable, and physiologically inert,[15] its use as a tissue substrate has been limited due to its relatively poor mechanical properties compared to synthetic polymers.[16] The mechanical properties of single fibrils can be drastically improved via individualization of the microfibrils into nanofibrils using a variety of methods such as mechanical treatment, acid hydrolysis, or catalyzed oxidation.[12−14] Cellulose nanofibrils are ca. 5−20 nm wide and 100−300 nm long[12,17] and thus are not continuous structures such as electrospun nanofibers, but they can be fabricated into 3-D scaffolds via freeze- or supercritical-drying or protonation of the carboxylate groups. The former two methods have poor durability in water and thus are not suitable for cell culture. On the other hand, the pH-stability of the hydrogels formed using the latter method is further strengthened by replacing the proton with metal ions.[18] The resulting material is a hydrogel, which is one of the most widely used polymer systems in tissue engineering. They consist of physically cross-linked polymer chains that are hydrophilic. The mechanical properties, such as elasticity, can be substantially altered depending on the polymer chemistry, cross-link density, and metal salt solution.[18] In addition, hydrogels can easily conform to the defect shape,

Received: February 11, 2014
Accepted: October 8, 2014
Published: October 8, 2014

making them ideal candidates for injectable wound-healing materials.[19]

Although nanocellulose is known to support cellular growth,[20] it lacks biorecognition sites such as proteins or growth factors that are needed for cell signaling and direction. In addition, cellular adhesion on the chemically similar alginate hydrogels has been limited.[21,22] The nanocellulose hydrogels contain many surface carboxylic acids, which are useful for covalent protein attachment using the carbodiimide coupling reaction.[16] In this work, we explored the covalent and physical adsorption of the protein fibronectin onto the hydrogel surface to improve cell adhesion. Carboxylated cellulose nanofibrils cross-linked with Ca^{2+} and Fe^{3+} with nearly an order of magnitude difference in storage moduli (3.4 and 32 kPa, respectively)[18] were investigated for their ability to support the growth of C3H10T1/2 fibroblasts.

MATERIALS AND METHODS

Materials. Deionized water with resistance ~18.2 MΩ was used in all experiments. Calcium nitrate tetrahydrate and iron(III) nitrate nonahydrate, N-(3-(dimethylamino)propyl)-N′-ethylcarbodiimide-(EDC), *N*-hydroxysuccinimide (NHS), 2-(N-morpholino) ethanesulfonic acid (MES), paraformaldehyde, Tween-20, and Triton X-100 were purchased from Sigma-Aldrich and used as received. Dulbecco Modified Eagle's Medium (DMEM), fetal bovine serum (FBS), bovine serum albumin (BSA), 0.25% trypsin-EDTA, phosphate buffered saline (PBS), micro-BCA protein assay kit, and antibiotic/antimycotic (Cellgro cat. 30-004-C1) were obtained from Fisher Scientific. Mouse mAb, clone 17 fibronectin antibody was obtained from Abcam. Horseradish peroxidase (HRP)-conjugated donkey antimouse immunoglobulins secondary antibody was obtained from Jackson ImmunoResearch Laboratories. Rhodamine phalloidin, Amplex Red Assay Kit, and Human Fibronectin (FN) were obtained from Life Techologies. C3H10T1/2 fibroblast cells were obtained from American Type Culture Collection and used at a passage number of 13. Aqueous dispersion of carboxylated cellulose nanofibrils (balanced with sodium ions) was provided courtesy of the USDA Forest Products Laboratory (Madison, Wisconsin). The cellulose nanofibrils (CNF) were produced from wood pulp using the TEMPO oxidation technique as has been previously described.[23]

Hydrogelation. CNF hydrogels were produced by addition of a metal salt solution to the CNF aqueous dispersion as has been described previously.[18] Briefly, the CNF dispersion was stirred to form a low viscosity liquid, degassed, and then an equal weight of a 50 mM aqueous solution of metal salt ($Ca(NO_3)_2$, or $Fe(NO_3)_3$) was added dropwise without stirring. The resulting hydrogel was soaked and rinsed with acidic water (pH = 3, Fe^{3+} hydrogels only) and then neutral water several times to remove unbound metal ions.

Protein Attachment. The hydrogels were thoroughly rinsed with PBS and cut to fit into 24-well plates. For the covalent attachment of protein, the substrates were immersed in a MES buffer containing of 5 mg/mL EDC and 5 mg/mL NHS for 1 h at RT. Substrates were rinsed with MES buffer and incubated in a 50 μg/mL fibronectin solution at 4 °C overnight. The protein solution was removed, and the substrates were washed in a 0.05% Tween 20 solution in PBS with gentle shaking for 30 min to remove physically absorbed protein. Previous research has shown that this process removes ca. 93% of physisorbed proteins.[24] Substrates with physically adsorbed proteins were prepared by immersing the hydrogels in a 50 μg/mL fibronectin solution at 4 °C overnight. Substrates were then washed thoroughly with PBS and sterilized overnight by immersing in a sterile solution of 2% antibiotic/antimycotic in PBS. Samples were kept sterile for cell culture studies or rinsed thoroughly with deionized water and dried for characterization.

Characterization of Substrates. The morphology of the hydrogels was examined using a field-emission scanning electron microscope (SEM, Hitachi S-4700) in the secondary-electron mode, using a mixture of upper and lower detectors. An accelerating voltage of 2 kV was maintained in order to prevent surface damage to the substrate. To prepare the specimens, the hydrogels were solvent-exchanged stepwise with acetone/H_2O (50:50), acetone/H_2O (75:25), and then with acetone for several times to completely remove water. The acetone gels were then supercritical CO_2-dried. Before observation, the samples were sputter coated with gold–palladium. Several areas were imaged in order to examine the uniformity of the nanofibril diameters. Nanofibril diameters were measured using image analysis software (ImageJ v 1.34, National Institutes of Health) and were not corrected for the sputter layer thickness. All samples were prepared and sputter coated at the same time.

Fourier transform infrared (FTIR) spectra of the dried samples of CNFs and the CNFs with protein were collected on a Thermo Nicolet NEXUS 870 spectrophotometer. The samples were obtained by freeze-drying the hydrogels. Sample pellets were prepared by grinding with KBr powder with the dried samples and pressing into pellets. The spectra were acquired in transmission mode on the sample pellets using 128 averaged scans and 4 cm^{-1} resolution over the spectral range 4000–400 cm^{-1}. Surface compositional analysis was performed using a PHI 5700 X-ray photoelectron spectroscopy (XPS) system equipped with a hemispherical analyzer. Samples were irradiated with a 400 W nonmonochromatic Al Kα (1486.6 eV) X-ray beam, and analysis was performed on sample areas of 2 mm × 0.8 mm with a takeoff angle of 45°. The XPS chamber pressure was maintained between 1×10^{-9} and 2×10^{-9} Torr. Elemental high resolution scans were conducted with a 23.5 eV pass energy for the C 1s, O 1s, and N 1s core levels. A value of 284.6 eV for the methylene component of the C 1s spectrum was used as the calibration energy for the binding energy scale, and all other spectra were shifted by the corresponding amount. Data were processed using Casa XPS software v 2.3.15.

Micro-BCA Assay. Quantification of protein was determined using a by difference assay. Gels with physically absorbed protein were prepared by soaking in protein overnight, rinsed twice with PBS and the removed protein solution and rinses were combined with an equal volume of working reagent. Gels with covalently attached protein were prepared by reacting with EDC/NHS, rinsing with buffer, and then soaking in a fibronectin solution overnight. To remove unbound protein, the gels were rinsed 30 min in a 0.05% Tween-20 solution and then in PBS. The protein soaking and rinse solutions were combined to serve as the final protein solution for analysis. An aliquot of the protein solution was diluted into an equal volume of working solution to serve as the initial protein solution. Samples were analyzed according to the manufacturer's instructions. The amount of protein attached per gel volume was determined by taking the difference between the initial and final protein concentrations, determined by a calibration curve.

Determination of Biological Activity of Substrate-Bound Fibronectin via ELISA. Nanocellulose gels with physically adsorbed and covalently attached fibronectin, as well as controls, were blocked with 5% donkey serum and 1% bovine serum albumin in PBS for 2 h at 4 °C, and then rinsed with PBS. The substrates were immersed in primary antibody solutions specific to FN (mouse mAb, clone 17, Abcam, 1:250 dilution) overnight at 4 °C. The substrates were rinsed with 0.05% Tween-20 in PBS for 30 min followed by PBS. The secondary antibody horseradish peroxidase (HRP)-conjugated donkey antimouse immunoglobulins (Jackson ImmunoResearch Laboratories) was diluted 1:10,000 in 5% donkey serum. The substrates were immersed for 3 h at RT and thoroughly rinsed with 0.05% Tween-20 in PBS followed by PBS. 100-μM Amplex Red reagent (10-acetyl-3,7-dihydroxyphenoxazine) and 20-μM H_2O_2 (Amplex Red assay kit, Invitrogen) prepared in sodium phosphate buffer (0.05 M, pH~ 7.4) were added to each sample well. The enzymatic reaction was allowed to proceed for 30 min at room temperature (RT) protected from light. Aliquots were taken from each sample well and transferred to a black 96-well assay plate with a clear glass bottom (Corning, Inc.). The fluorescence intensity was measured using a PerkinElmer Universal Microplate Analyzer (Waltham, MA) with a 538 nm excitation filter. The enzymatic activity of HRP was correlated to the biological activity of substrate-bound protein epitopes following normalization to the dry

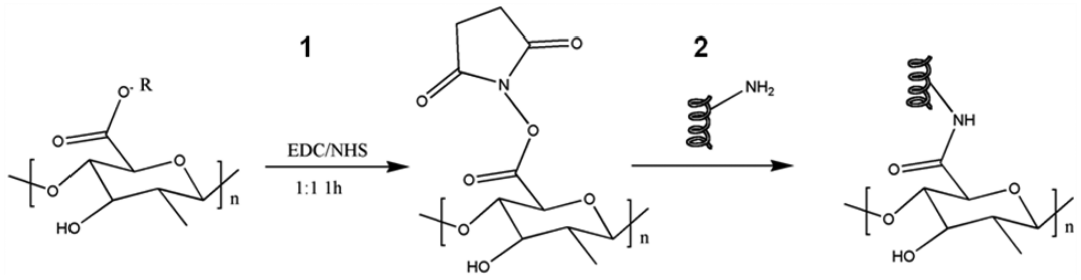

Figure 1. Schematic of covalent coupling reaction for the attachment of protein to nanocellulose hydrogels. (1) Attachment of NHS via EDC coupling reaction (5 mg/mL, 1:1). (2) Attachment of protein through reaction with amine groups. R denotes H^+, Ca^{2+}, or Fe^{3+}.

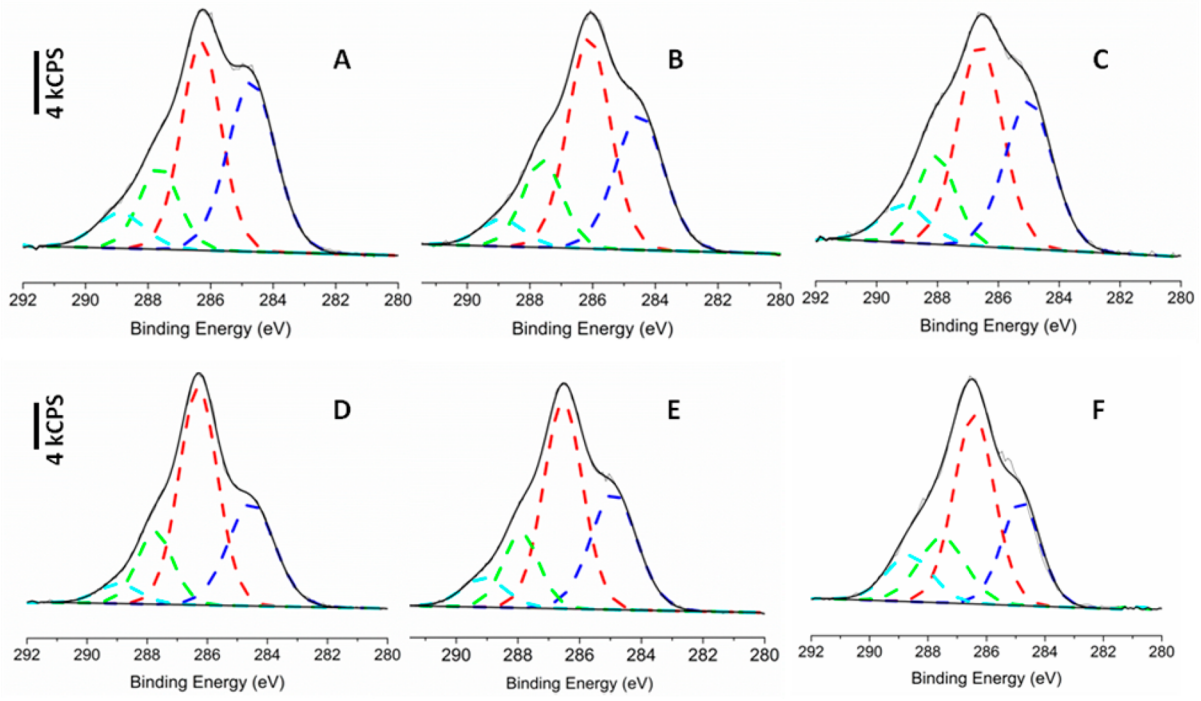

Figure 2. High-resolution X-ray photoelectron spectra of nanocellulose hydrogels. (A) C 1s of unmodified Ca^{2+} nanocellulose hydrogel, (B) C 1s of Ca^{2+} nanocellulose hydrogel with physically adsorbed fibronectin, (C) C 1s of Ca^{2+} nanocellulose hydrogel with covalently attached fibronectin, (D) C 1s of unmodified Fe^{3+} nanocellulose hydrogel, (E) C 1s of Fe^{3+} nanocellulose hydrogel with physically adsorbed fibronectin, (F) C 1s of Fe^{3+} nanocellulose hydrogel with covalently attached fibronectin. The components are C1 (blue), C2 (red), C3 (green), and C4 (cyan).

weight of the gel. A minimum of three test samples (n = 3) were analyzed for each protein-modified substrate.

Culture of Fibroblast Cells. C3H10T1/2 cells were used to study the ability of the nanocellulose hydrogels to act as tissue substrates. The cells were cultured in DMEM medium supplemented with 10% FBS and 1% antibiotic/antimycotic at 37 °C and 5% CO_2. Sterile substrates in 24-well plates were incubated in serum-free medium 2 h prior to seeding cells. C3H10T1/2 cells were removed from the growth flask with 0.25% trypsin and seeded on the gels at a density of 5000 cells/well in a 24 well plate in 1% FBS in DMEM. Cells were allowed to attach to the gel for 2 h before adding 1 mL of medium to each well.

After day 5 of culture, cellular coverage and spreading was characterized by staining actin filaments with phalloidin and analyzing with confocal laser scanning microscopy (CLSM). To prepare samples for CLSM, the substrates were rinsed thoroughly with PBS and fixed in 4% paraformaldehyde in PBS for 20 min. Substrates were rinsed with PBS and cells were permeabilized with 0.2% Triton X-100 for 10 min. Nonspecific labeling was prevented by incubating samples in a blocking buffer composed of 1% BSA in PBS for 20 min. Samples were then immersed in rhodamine phalloidin (1:200) in blocking buffer for 1 h. Samples were rinsed thoroughly with PBS and kept in the dark at 4 °C until analysis. Samples were imaged on a Zeiss LSM5 Pascal equipped with Epiplan-Neofluar lenses. The cells on the substrates were imaged with a 543 nm laser. A minimum of n = 5 random areas for each of 3 replicate samples were imaged using the 10× and 20× objectives. The cell coverage was determined by an image area analysis of CLSM images using ImageJ software.

Statistics. All data are expressed as mean ± standard deviation (SD) unless noted. Unpaired Student's t tests were conducted with a significance level of $p < 0.05$ using Origin v 8.5.

RESULTS

The diffusion of metal cations into the CNF suspension induced rapid gelation, as we have previously described.[18] The gels held their shape well and were mechanically robust enough to cut to fit in well plates and transfer for analysis. To improve the cellular adhesion of the substrates, the ECM protein fibronectin was attached either via physical adsorption or covalent attachment. Figure 1 shows the scheme for covalent attachment using a carbodiimide coupling reaction.

The oxidized nanofibrils contained surface carboxylate groups that were activated with EDC/NHS and coupled to the protein. It was expected that these samples would better

serve as long-term cell culture platforms compared to substrates with physically adsorbed proteins because the proteins would not leach from the surface over time. However, the covalent attachment could potentially lock the protein in a biologically inactive conformation. In addition, potentially less protein could attach to the surface due to steric hindrance issues. Thus, both methods of protein attachment were examined to determine the optimal protein attachment mechanism.

The gels were freeze-dried, and protein attachment was characterized by XPS and FTIR. While both characterization methods are qualitative in nature, XPS revealed information about the relative amount of protein on the surface whereas FTIR provided information about the protein content throughout the entire gel. Figure 2 displays the high resolution XPS C 1s spectra for Ca^{2+} and Fe^{3+} cross-linked hydrogels. The C 1s envelope consisted of 4 major components (with increasing binding energies): the hydrocarbon (C1), hydroxyl carbon (C2), carbonyl carbon/amide carbon (C3), and the carboxylic acid (C4).[13,25]

The atomic composition of the native and surface-modified hydrogels is displayed in Table 1. The hydrogel controls consisted of carbon, oxygen, and the metal ion used to cross-link the gel. Nitrogen was also observed for the gels with attached protein. The highest nitrogen-to-carbon ratio (N/C), indicative of the relative quantity of protein on the surface, was observed on the Ca^{2+} gel with covalently attached protein, followed by the Fe^{3+} gel with covalently attached protein. The gels with physically adsorbed protein had significantly lower nitrogen-to-carbon ratios, with the ratio for the Ca^{2+} gel higher than for the Fe^{3+} gel. A small amount of nitrogen was observed on the Fe^{3+} control gel, most likely due to insufficient rinsing of the iron nitrate salt used for hydrogelation.

Table 1. Atomic Composition of Native and Modified Nanocellulose Hydrogels As Determined by X-ray Photoelectron Spectroscopy

	XPS atomic percentage[a]					
surface chemistry	C	O	N	Ca^{2+}	Fe^{3+}	N/C[a] 100
Ca^{2+} control	53.7	45.8		0.5		0
Ca^{2+} w/physisorbed fibronectin	56.8	40.6	2.4	0.2		4.3
Ca^{2+} w/covalently attached fibronectin	57.8	36.3	5.8	0.1		10.0
Fe^{3+} control	51.6	47.0	0.4		1.0	0.8
Fe^{3+} w/physisorbed fibronectin	54.7	43.7	0.9		0.7	1.6
Fe^{3+} w/covalently attached fibronectin	54.7	40.3	4.3		0.7	7.8

[a]Some contaminants were observed (Na, Cl, Si) and were not included in the calculations in the table.

The chemical composition of the carbon peak is shown in Table 2. In general, the carboxylic acid (C4) component increased with the addition of protein, most likely due to the addition of aspartic acid side chains (although some of the carboxylic acids were converted into amide bonds). Likewise, the amide component (C3) increased for the substrates with covalently attached protein.

The chemical composition was also evaluated using FTIR. The results are displayed in Figure 3 and Table 3. Peak fitting of the υ_{as}OCO band at ~1615 cm^{-1} revealed three components for the native Ca^{2+} and Fe^{3+} nanocellulose hydrogels, and a fourth components for an amide II band (P1, blue ~1550 cm^{-1}) in the protein-modified gels.[26] The component at ~1605 cm^{-1} (P2, red) represents the O−C−O asymmetric stretching.[18] The component at ~1650 cm^{-1} (P3, green) corresponds to the amide I band as well as adsorbed hydroxyl groups (from water).[26−28] The component at ~1720 cm^{-1} (P4, cyan) denotes the carboxylic acid.[29] The amide II composition (P1) increased with the addition of protein and was highest for the Fe^{3+} cross-linked gels with covalently attached protein. There was also, in general, a slight increase in the amide I (P3) with increased protein addition, but this is partially masked by the adsorbed water. The carboxylic acid component (P4) increased slightly for the gels with covalently attached protein.

Table 2. Carbon Chemical Composition of Native and Modified Nanocellulose Hydrogels As Determined by X-ray Photoelectron Spectroscopy

	XPS C 1s percentage			
surface chemistry	C1	C2	C3	C4
Ca^{2+} control	38.1	38.7	15.2	8.1
Ca^{2+} w/physisorbed fibronectin	34.6	50.0	9.0	6.4
Ca^{2+} w/covalently attached fibronectin	22.5	50.4	15.7	11.4
Fe^{3+} control	29.0	50.4	15.6	5.0
Fe^{3+} w/physisorbed fibronectin	24.0	50.9	15.6	9.5
Fe^{3+} w/covalently attached fibronectin	23.9	45.4	18.2	12.5

Quantification of the protein using a BCA assay was probed using a by difference assay as described above. The Fe^{3+} gels with physically adsorbed protein has 19.2 ± 7.5 $\mu g/cm^3$ protein attached, whereas the Ca^{2+} gel with physically adsorbed protein had 22.5 ± 6.5 $\mu g/cm^3$ protein attached. Quantification of the gels with covalently attached protein was not possible due to interference attributed to the *N*-hydroxysuccinimide. An enzyme-linked immunosorbent assay (ELISA) was used to measure the biological activity per mg of dry gel as shown in Table 4. For this assay, the FN monoclonal antibody A17 was used, which has a high affinity for the 120-kDa cell-binding domain that encompasses the central RGD integrin-binding motif. The highest relative bioactivity was observed on the Ca^{2+} gel with covalently attached fibronectin, which correlates well with the XPS and FTIR data. However, the Fe^{3+} gel with covalently attached fibronectin had lower bioactivity than the substrates with physically adsorbed protein, although it had more protein attached according to XPS and FTIR.

After surface modification, the gels were solvent-exchanged with acetone followed by supercritical CO_2 drying prior to SEM analysis. This drying process was found to best preserve the morphology of the nanofibrils for the SEM studies. A fine network of interconnected nanofibrils with open pore structures was observed for both control and protein-modified gels (see Figure 4). Nanofibril diameters were measured using ImageJ software and ranged from 16 to 23 nm with the coating, which is in the range of single nanofibrils. The pore size of the surface layer is 94.9 ± 51 nm, measured from SEM images. In all cases except for the Fe^{3+} gels with covalently attached protein, the diameters were significantly larger for the protein-modified fibrils ($p < 0.05$). Moreover, the fibril diameters for the Ca^{2+} gel with covalently attached protein were significantly larger than those of the gels with the physically adsorbed protein ($p < 0.05$).

After verifying protein attachment and the preservation of the nanofibril size and hydrogel porosity, the cell adhesive properties of the substrates were probed with fibroblast cells. Fibroblasts synthesize precursors to the ECM and collagen,

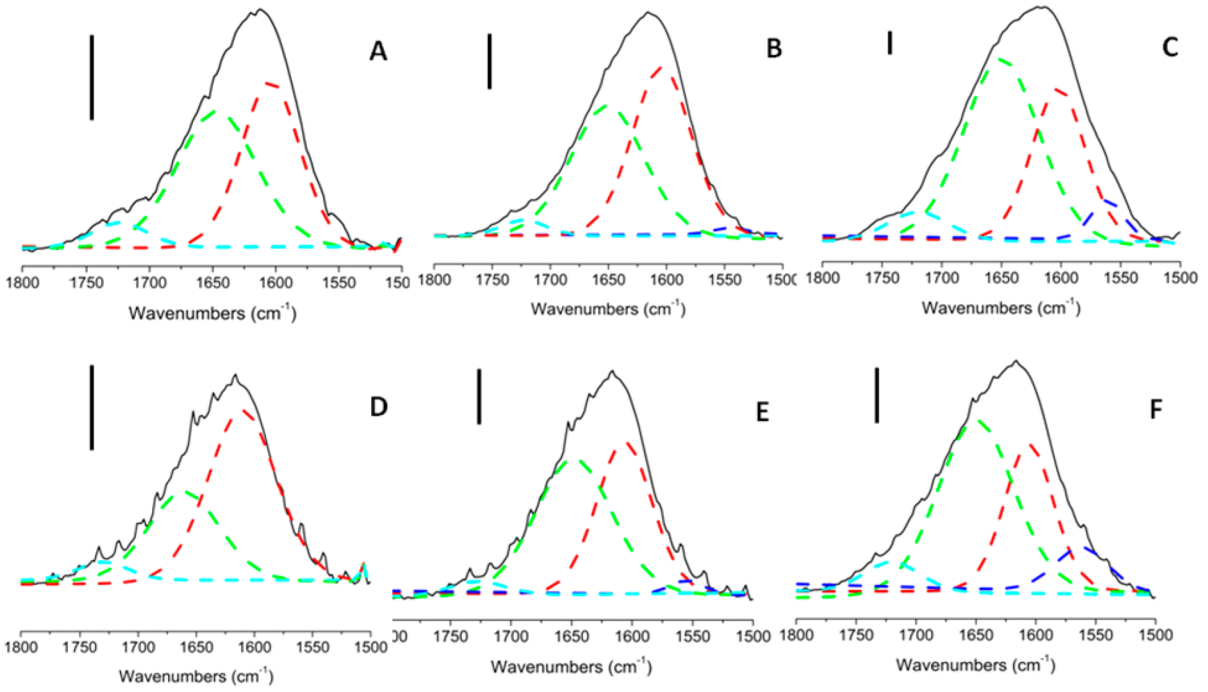

Figure 3. FTIR spectra of υ_{as}OCO band at 1615 cm^{-1} for nanocellulose hydrogels. (A) unmodified Ca^{2+} nanocellulose hydrogel, (B) Ca^{2+} nanocellulose hydrogel with physically adsorbed fibronectin, (C) Ca^{2+} nanocellulose hydrogel with covalently attached fibronectin, (D) C 1s of unmodified Fe^{3+} nanocellulose hydrogel, (E) Fe^{3+} nanocellulose hydrogel with physically adsorbed fibronectin, (F) Fe^{3+} nanocellulose hydrogel with covalently attached fibronectin. Scale bar denotes 0.045 absorbance units.

Table 3. Chemical Composition of υ_{as}OCO Band at 1615 cm^{-1} for Nanocellulose Hydrogels as Determined by FTIR

	FTIR 1615 cm^{-1} peak fitting percentage			
surface chemistry	P1	P2	P3	P4
Ca^{2+} control		44.4	49.3	6.3
Ca^{2+} w/physisorbed fibronectin	1.1	48.4	47.1	3.3
Ca^{2+} w/covalently attached fibronectin	5.1	32.3	55.4	7.1
Fe^{3+} control		61.6	33.5	4.9
Fe^{3+} w/physisorbed fibronectin	2.4	41.7	52.1	3.8
Fe^{3+} w/covalently attached fibronectin	9.7	29.5	53.9	6.9

Table 4. Biological Activity of Fibronectin Protein as Determined by ELISA[a]

surface chemistry	relative bioactivity per mg of substrate (AU)
Ca^{2+} w/physisorbed fibronectin	0.136 ± 0.001
Ca^{2+} w/covalently attached fibronectin	0.325 ± 0.23
Fe^{3+} w/physisorbed fibronectin	0.199 ± 0.25
Fe^{3+} w/covalently attached fibronectin	0.017 ± 0.03

[a]Fluorescence was corrected by subtracting control values and normalized to the dry weight of the nanocellulose gel, $n = 4$.

maintain the structural integrity of connective tissue, and play an important role in wound healing, and thus, they are a suitable cell line to evaluate the efficacy of CNF as tissue substrates. Cellular attachment and spreading of fibroblasts was accessed after 5 days. This time point was found to be optimal for accessing the effects of substrate chemistry based on previous cellular assays. Attachment studies have been assessed by others at a wide range of time points from as short as 4 h to

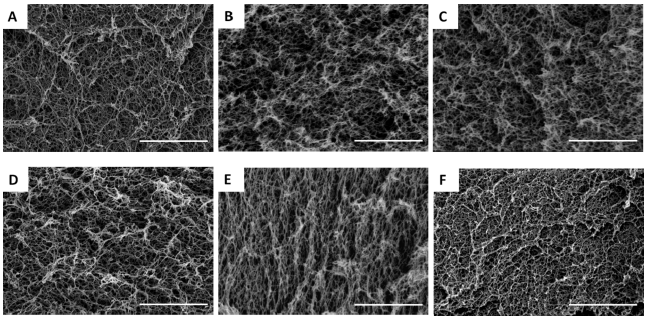

Figure 4. Scanning electron microscopy images of Ca^{2+} and Fe^{3+} cross-linked nanocellulose hydrogels. (A) Unmodified Ca^{2+} nanocellulose hydrogel, (B) Ca^{2+} nanocellulose hydrogel with physically adsorbed fibronectin, (C) Ca^{2+} nanocellulose hydrogel with covalently attached fibronectin, (D) unmodified Fe^{3+} nanocellulose hydrogel, (E) Fe^{3+} nanocellulose hydrogel with physically adsorbed fibronectin, (F) Fe^{3+} nanocellulose hydrogel with covalently attached fibronectin. Scale bar denotes 2 μm.

18 days.[22,30,31] Although several different time points would have been helpful in understanding cellular attachment and proliferation kinetics, a single time point still allowed evaluation and comparison of the cellular attachment and spreading on each of the six different substrates and one of the first evidence that demonstrate the use of metal cation cross-linked nanocellulose as cell culture substrates.

Figure 5 displays representative images of C3H10T1/2 cells grown on the hydrogels for 5 days. Very little cellular infiltration into the 3D hydrogels was observed, most likely due to the nanometer-sized pores. The unmodified Ca^{2+} nanocellulose hydrogel (Figure 5 A) appears to be the least favorable for cell attachment and spreading. Very few cells are attached, and the cells have a predominantly round shape,

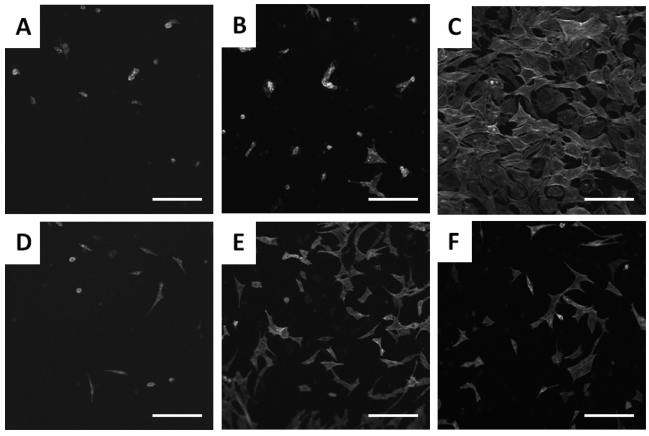

Figure 5. Confocal laser scanning images of C3H10T1/2 cells on Ca^{2+} and Fe^{3+} cross-linked nanocellulose hydrogels. (A) unmodified Ca^{2+} nanocellulose hydrogel, (B) Ca^{2+} nanocellulose hydrogel with physically adsorbed fibronectin, (C) Ca^{2+} nanocellulose hydrogel covalently attached fibronectin, (D) unmodified Fe^{3+} nanocellulose hydrogel, (E) Fe^{3+} nanocellulose hydrogel with physically adsorbed fibronectin, (F) Fe^{3+} nanocellulose hydrogel with covalently attached fibronectin. Scale bar denotes 200 μm.

indicating little interaction or contact with the surface. A similar number of cells attached to the Ca^{2+} nanocellulose hydrogel with physically adsorbed fibronectin (Figure 5 B), but there is an increased percentage of cells spreading or extending their cytoplasm and deviating from round morphology. The cells behaved much differently on the Ca^{2+} nanocellulose hydrogel with covalently attached protein (Figure 5 C)—a very dense layer of spread cells covered the surface. Overall, the spreading of the cells on the Fe^{3+} nanocellulose hydrogels was improved compared to the Ca^{2+} cross-linked gels (Figure 5 D–F). Very few cells with round morphology were observed on the Fe^{3+} gels, particularly those with attached protein. The number of cells attached on the Fe^{3+} nanocellulose hydrogels was improved with protein attachment albeit not drastically. The cellular coverage, determined by an image analysis of the fraction of the image occupied with cells and indicative of the number of cells adhered and degree of cellular spreading, was also examined. Cellular coverage increased with protein modification, but unlike the Ca^{2+} cross-linked gels, the highest coverage occurred on the Fe^{3+} gels with physically adsorbed protein. Indeed, very low cell coverage was observed on all except the Ca^{2+} gels with covalently attached protein and the Fe^{3+} gels with physically adsorbed protein (see Figure 6A). The percentage of spread cells was improved in all cases with the attachment of protein (Figure 6 B). The percentage of cells spread was fairly high for all of the Fe^{3+} gels, ranging from 68.1 ± 13.5% for the unmodified gel to 92.5 ± 11.2% for the gel with physically adsorbed protein. For the Ca^{2+} gels, the percentage of spread cells ranged from 14.4 ± 10.8% for the unmodified gel to 97.9 ± 3.9% for the gel with covalently attached protein. The gels with the highest percentage of spread cells followed the same trend as the number of cells adhered, with the Ca^{2+} gels with covalently attached protein and the Fe^{3+} gels with physically adsorbed protein being most favorable for cellular extension.

DISCUSSION

In this work, we were interested in probing the efficacy of nanocellulose hydrogels cross-linked with either Ca^{2+} or Fe^{3+} as

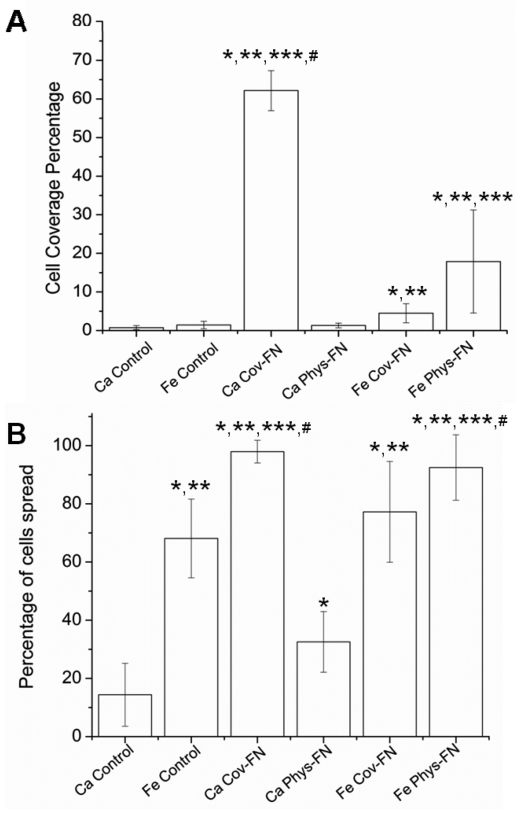

Figure 6. Interaction of C3H10T1/2 cells on Ca^{2+} and Fe^{3+} cross-linked nanocellulose hydrogels. (A) Cellular coverage as determined by image area analysis. Error bars denote mean ± standard deviation (*p < 0.05 compared to controls, **p < 0.05 compared to Ca^{2+} Phys-FN, *** p < 0.05 compared to Fe^{3+} Cov-FN, #p < 0.05 compared to Fe^{3+} Phys-FN). (B) Percentage of cells deviating from round morphology. Error bars denote mean ± standard deviation (*p < 0.05 compared to Ca^{2+} control, **p < 0.05 compared to Ca^{2+} Phys-FN, ***p < 0.05 compared to Fe^{3+} Control, #p < 0.05 compared to Fe^{3+} Cov-FN). Ca^{2+} control = unmodified Ca^{2+} nanocellulose hydrogel; Ca^{2+} Phys-FN = Ca^{2+} nanocellulose hydrogel with physically adsorbed fibronectin; Ca^{2+} Cov-FN = Ca^{2+} nanocellulose hydrogel with covalently attached fibronectin; Fe^{3+} Control = unmodified Fe^{3+} nanocellulose hydrogel; Fe^{3+} Phys-FN = Fe^{3+} nanocellulose hydrogel with physically adsorbed fibronectin; Fe^{3+} Cov-FN = Fe^{3+} nanocellulose hydrogel with covalently attached fibronectin.

tissue engineering substrates. Due to the low cellular adhesion observed on native polysaccharide materials (alginate),[21,22] we explored a method to modify the surface with protein. The XPS results suggested that the Ca^{2+} and Fe^{3+} gels with covalently attached protein had the highest protein surface concentrations. Thus, the highest levels of cellular attachment and spreading were expected on these materials due to the high concentration of biomolecules such as arginine−-glycine−aspartic acid (RGD) cell-adhesive motifs. The cellular assay, which directly probes bioactive protein on the surface, confirmed this trend only for the Ca^{2+} gel, which had the highest cell coverage and percentage of spread cells. However, the ELISA suggested that less of the protein covalently attached on the Fe^{3+} gels was biologically active, compared to the other protein-modified gels, providing a possible explanation for the reduced cellular adhesion on this substrate. The cellular coverage was significantly lower for all of the Fe^{3+} gels compared to the Ca^{2+} gel with covalently attached protein. In addition, the Fe^{3+} substrates with physically adsorbed protein (and significantly

lower N/C ratio) had significantly higher coverage and percentage of spread cells compared to the Fe^{3+} substrates with covalently attached protein and the Ca^{2+} with physically adsorbed protein. The ELISA showed higher protein bioactivity for the Fe^{3+} substrates with physically adsorbed protein compared to covalently attached protein but similar bioactivity to the Ca^{2+} gels with physically adsorbed protein.

Machida-Sano et al. has reported differences in hydrophobicity of Ca^{2+} and Fe^{3+} cross-linked alginate gels, with the latter being more hydrophobic and having a better adsorption of serum proteins such as vitronectin.[21] Higher levels of cell adhesion were observed on the Fe^{3+} substrates compared to Ca^{2+} substrates with physically adsorbed proteins such as in the aforementioned study, which is in agreement with our results. The percentage of fibroblast cells spread ranged from 14.3% to 88.5% on the iron cross-linked alginate gels with 5 μg/mL fibronectin and 5 μg/mL fibronectin with 5 μg/mL vitronectin, respectively. We observed similar levels of spread cells on Fe^{3+} cross-linked nanocellulose gels with physically adsorbed fibronectin to the latter sample (92.5 $\pm$ 11.2%). It should be noted though that besides using a different polysaccharide matrix, our samples were treated with an order of magnitude higher concentration of fibronectin (50 μg/mL) and all cellular assays were done in the presence of 1% FBS which contains vitronectin.

Although the cellular assay was done in low serum conditions (1% FBS), as mentioned above there was still a small amount of serum proteins present that could have adsorbed preferentially on the surface of the Fe^{3+} gels during culturing, thus improving the favorability of the Fe^{3+} substrates over the Ca^{2+} for cell attachment in general. However, we found from the ELISA that the conformation of proteins on Fe^{3+} gel with covalently attached protein was less bioactive compared to the physically adsorbed conformations. Zhang et al. has reported reduced activity of covalently attached fibronectin on aminated polyethylene terephthalate due to fibrillogenesis and blocked access of the RDG motifs. Consequently, cell adhesion was improved on the surfaces with physically adsorbed fibronectin.[32] However, the Ca^{2+} gel with physically adsorbed protein had a high XPS N/C ratio, and similar bioactivity as determined by the ELISA, but very little cell attachment and spreading. Possibly reduced serum protein adsorption caused decreased cellular adhesion. Salmerón-Sánchez et al. found that fibronectin fibrillogenesis and resulting bioactivity can be controlled by chemistry of the substrate surface. In some cases, the fibrillated fibronectin exhibited higher bioactivity compared to the globulin form.[33] The influence of material surface chemistry and protein attachment mechanisms play an important yet complex role in the resulting bioactivity of the attached protein.

Based on our previous FTIR analysis, Fe^{3+} gels were expected to have more free carboxylic acid groups to covalently bind protein,[18] but less protein was attached compared to the Ca^{2+} gels based on XPS results. Transmission FTIR, which probes the bulk chemical information, suggested similar amounts of protein in both gels based on fitting of the amide I and amide II bands. Thus, the protein is potentially binding differently to the Fe^{3+} gels and cross-linking two or more fibrils, rather than binding to a single fibril. If this was the case, there could potentially be less protein detected in the uppermost surface of the gel.

Based on our previous modeling, the binding energy of trivalent cations was significantly higher than for divalent ions.[18] Thus, Fe^{3+} ions are expected to be more difficult to replace in the protein coupling reaction, which is confirmed by the smaller relative decrease in Fe content after protein attachment compared to Ca content as determined by XPS. The trivalent ions such as Fe^{3+} are predicted to form complexes with 2 or 3 fibrils, whereas the divalent ions like Ca^{2+} form either intrafibril cross-links or cross-links between 2 fibrils, which accounts for the differences in modulus observed.[18] Thus, if there is a high concentration of interfibril cross-linking, the fibrils will be slightly closer together in the Fe^{3+} gels, which could mean potentially different binding conformations for the protein. As discussed previously, the protein may be binding to multiple fibrils in close proximity rather than a single fibril. Therefore, the protein may have a different conformation and resulting bioactivity and could account for varied surface concentrations of protein observed. In the case of physically adsorbed protein, the counterion need not be replaced, and thus the protein may take on a different conformation and corresponding bioactivity based on the local hydrophobic and electrostatic forces. In addition, the effects of metal ion chelation, particularly for Fe^{3+} could play an important role in protein conformation and bioactivity. Due to the ca. 100 nm pore size, minimal cell infiltration occurred and thus the 3D gel essentially acted as a 2D substrate. Thus, the amount of surface protein as determined by XPS is perhaps more relevant than the FTIR analysis, although, certainly, the most relevant assays were the ELISA and cellular assays, which probed the amount of protein in its biologically active form.

Our studies focused on in vitro assays in order to gain a basic understanding of how cells might respond to nanocellulose wound dressings in vivo. Fibroblasts are widely used in in vitro studies to assess cellular attachment. Certainly, in vitro conditions do not replicate in vivo situations due to a great number of factors that would have to be taken into consideration. However, in vitro assays are useful to screen new biomaterials, thereby limiting the number of in vivo assays.

CONCLUSIONS

Nanocellulose hydrogels were fabricated from wood pulp using a TEMPO oxidation technique and then gelled by the addition of metal salts. The hydrogels were then modified with the ECM protein fibronectin to improve their cell adhesive properties for use as tissue substrates. C3H10T1/2 cells were grown on the surface for 5 days, and the best cellular attachment and spreading was observed on the Ca^{2+} cross-linked gels with covalently attached protein, followed by the Fe^{3+} cross-linked gels with physically adsorbed protein. The cellular adhesion was minimal on unmodified hydrogels, and in all cases, it was improved with the attachment of protein. The percentage of cells spread was higher for Fe^{3+} cross-linked gels compared to the Ca^{2+} gels (except for the Ca^{2+} gel with covalently attached protein), possibly due the increased hydrophobicity and greater adsorption of serum proteins.

Due to the nanometer size pores in the nanocellulose hydrogels, minimal cellular infiltration was anticipated. Thus, the cells were expected to remain predominantly on the surface of the gels. Indeed, we observed minimal penetration into the nanoporous network with cells infiltrating only in the top ca. 50 to 100 μm of the substrate. In order for cells to truly infiltrate into a substrate and form complex tissue, the pore sizes need to be on the order of the cell body diameter.[34] Thus, new methods are needed to increase the porosity of the hydrogels if such materials are to be used for this purpose. In their current state,

the hydrogels still possess many of the desired characteristics for a tissue substrate and with protein modification successfully supported the growth of fibroblasts. Thus, these hydrogels are suitable for biomedical applications in which cellular infiltration is less critical such as bandages or wound healing materials. In addition, due to their high surface area and porosity, they could also find applications in drug delivery, filtration, and catalysis. Additional biological/medical applications of nanocellulose are expected, too, due to the natural abundance and low-cost of their production compared to other biocompatible polymers.

AUTHOR INFORMATION

Corresponding Author

*Phone: 410-306-1965. Fax 410-306-0676. E-mail: nicole.e.zander.civ@mail.mil.

Author Contributions

The manuscript was written through contributions of all authors. All authors have given approval to the final version of the manuscript.

Notes

The authors declare no competing financial interest.

ACKNOWLEDGMENTS

The authors thank Dr. Alan Rudie and Mr. Richard Reiner at USDA Forest Product Laboratory (FPL) for providing CNF dispersions.

REFERENCES

(1) Shi, J.; Wang, L.; Zhang, F.; Li, H.; Lei, L.; Liu, L.; Chen, Y. Incorporating Protein Gradient into Electrospun Nanofibers as Scaffolds for Tissue Engineering. *ACS Appl. Mater. Interfaces* **2010**, *2*, 1025−1030.

(2) Chan, B. P.; Leong, K. W. Scaffolding in Tissue Engineering: General Approaches and Tissue-Specific Considerations. *Eur. Spine J.* **2008**, *17*, 467−479.

(3) Ratner, B. D.; Hoffman, A. S.; Schoen, F. S.; Lemons, J. E. *Biomaterials Science*; Elsevier Science: San Diego, 1996; pp 5−6.

(4) Neal, R. A.; McClugage, S. G.; Link, M.C.; Sefcik, L. S.; Ogle, R. C.; Botchwey, E. A. Laminin Nanofiber Meshes that Mimic Morphological Properties and Bioactivity of Basement Membranes. *Tissue Eng., Part C* **2009**, *15*, 11−21.

(5) Discher, D. E.; Mooney, D. J.; Zandstra, P. W. Growth Factors, Matrices, and Forces Combine and Control Stem Cells. *Science* **2009**, *324*, 1673−1677.

(6) Li, W.; Laurencin, C. T.; Caterson, E. J.; Taun, R. S.; Ko, F. K. J. Electrospun Nanofibrous Structure: a Novel Scaffold for Tissue Engineering. *Biomed. Mater. Res.* **2002**, *60*, 613−621.

(7) Lutolf, M. P.; Hubbell, J. A. Synthetic Biomaterials as Instructive Extracellular Microenvironments for Morphogenesis in Tissue Engineering. *Nat. Biotechnol.* **2005**, *23*, 47−55.

(8) Venugopal, J.; Low, S.; Choon, A. T.; Ramakrishna, S. Interaction of Cells and Nanofiber Scaffolds in Tissue Engineering. *J. Biomed. Mater. Res., Part B* **2008**, *84B*, 34−48.

(9) Ekaputra, A. K.; Prestwich, G. D.; Cool, S. M.; Hutmacher, D. W. Combining Electrospun Scaffolds with Electrosprayed Hydrogels Leads to Three-Dimensional Cellularization of Hybrid Constructs. *Biomacromolecules* **2008**, *9*, 2097−2103.

(10) Thorvaldsson, A.; Stenhamre, H.; Gatenholm, P.; Walkenstrom, P. Electrospinning of Highly Porous Scaffolds for Cartilage Regeneration. *Biomacromolecules* **2008**, *9*, 1044−1049.

(11) Kumbar, S. G.; James, R.; Nukavarapu, S. P.; Laurencin, C. T. Electrospun Nanofiber Scaffolds: Engineering Soft Tissues. *Biomed. Mater.* **2008**, *3*, 034002−034016.

(12) Szczęsna-Antczak, M.; Kazimierczak, J.; Antczak, T. Nanotechnology—Methods of Manufacturing Cellulose Nanofibres. *Fibres Text. East. Eur.* **2012**, *20*, 8−12.

(13) Barazzouk, S.; Daneault, C. Spectroscopic Characterization of Oxidized Nanocellulose Grafted with Fluorescent Amino Acids. *Cellulose* **2011**, *18*, 643−653.

(14) Kamel, S. Nanotechnology and its Applications in Lignocellulosic Composites, a Mini Review. *Express Polym. Lett.* **2007**, *9*, 546−575.

(15) Peterson, N.; Gatenholm, P. Bacterial Cellulose-Based Materials and Medical Devices: Current State and Perspectives. *Appl. Microbiol. Biotechnol.* **2011**, *91*, 1277−1286.

(16) Anirudhan, T. S.; Rejeena, S. R.; Tharun, A. R. Investigation of the Extraction of Hemoglobin by Adsorption onto Nanocellulose-Based Superabsorbent Composite Having Carboxylate Functional Groups from Aqueous Solutions: Kinetic, Equilibrium, and Thermodynamic Profiles. *Ind. Eng. Chem. Res.* **2013**, *52*, 11016−11028.

(17) Gao, C.; Wan, Y.; Yang, C.; Dai, K.; Tang, T.; Luo, H.; Wang, J. Preparation and Characterization of Bacterial Cellulose Sponge with Hierarchical Pore Structure as Tissue Engineering Scaffold. *Porous Mater.* **2011**, *18*, 139−145.

(18) Dong, H.; Snyder, J. F.; Williams, K. S.; Andzelm, J. W. Cation-Induced Hydrogels of Cellulose Nanofibrils with Tunable Moduli. *Biomacromolecules* **2013**, *14*, 3338−3345.

(19) Hartwell, R.; Leung, V.; Chavez-Munoz, C.; Nabai, L.; Yang, H.; Ko, F.; Ghahary, A. A Novel Hydrogel-Collagen Composite Improves Functionality of an Injectable Extracellular Matrix. *Acta Biomaterialia* **2011**, *7*, 3060−3069.

(20) Bhattacharya, M.; Malinen, M. M.; Lauren, P.; Lou, Y.; Kuisma, S. W.; Kanninen, L.; Lille, M.; Corlu, A.; GuGuen-Guillouzo, C.; Ikkala, O.; Laukkanen, A.; Urtti, A.; Yliperttula, M. Nanofibrillar Cellulose Hydrogel Promotes Three-Dimensional Liver Cell Culture. *J. Controlled Release* **2012**, *164*, 291−298.

(21) Machida-Sano, I.; Matsuda, Y.; Namiki, H. In Vitro Adhesion of Human Dermal Fibroblasts on Iron Cross-Linked Alginate Films. *Biomed. Mater.* **2009**, *4*, 025008−025015.

(22) Machida-Sano, I.; Ogawa, S.; Ueda, H.; Kimura, Y.; Satoh, N.; Namiki, H. Effects of Composition of Iron-Cross-Linked Alginate Hydrogels for Cultivation of Human Dermal Fibroblasts. *Int. J. Biomater.* **2012**, *2012*, 820513−820521.

(23) Saito, T.; Kimura, S.; Nishiyama, Y.; Isogai, A. Cellulose Nanofibers Prepared by TEMPO-Mediated Oxidation of Native Cellulose. *Biomacromolecules* **2007**, *8*, 2485−2491.

(24) Zander, N. E.; Beebe, T. P. Immobilized Laminin Concentration Gradients on Electrospun Fiber Scaffolds for Controlled Neurite Outgrowth. *Biointerphases* **2014**, *9*, 0110031−0110039.

(25) Crist, B. V. *Handbook of Monochromatic XPS Spectra: Polymers and Polymers Damaged by X-rays*; John Wiley and Sons, LTD: West Sussex, England, 2000; p 48−50.

(26) Cheng, S.; Chittur, K. K.; Sukenik, C. N.; Culp, L. A.; Lewandowska, K. J. The Conformation of Fibronectin on Self-Assembled Monolayers with Different Surface Composition: an FTIR/ATR Study. *J. Colloid Interface Sci.* **1994**, *162*, 135−143.

(27) Morán, J. I.; Alvarez, V. A.; Cyras, V. P.; Vázquez, A. Extraction of Cellulose and Preparation of Nanocellulose from Sisal Fibers. *Cellulose* **2008**, *15*, 149−159.

(28) Oh, S. Y.; Yoo, D. I.; Shin, Y.; Seo, G. FTIR Analysis of Cellulose Treated with Sodium Hydroxide and Carbon Dioxide. *Carbohydr. Res.* **2005**, *340*, 417−428.

(29) Lasseuguette, E. Grafting onto Microfibrils of Native Cellulose. *Cellulose* **2008**, *15*, 571−580.

(30) Hamilton, V.; Yuan, Y.; Rigney, D. A.; Puckett, A. D.; Ong, J. L.; Yang, Y.; Elder, S. H.; Bumgardner, J. D. Characterization of Chitosan Films and Effects on Fibroblast Cell Attachment and Proliferation. *J. Mater. Sci. Mater. Med.* **2006**, *17*, 1373−1381.

(31) Mustafa, K.; Silva Lopez, B.; Hultenby, K.; Wennerberg, A.; Arvidson, K. Attachment and Proliferation of Human Oral Fibroblasts to Titanium Surfaces Blasted with Tio2 Particles. A Scanning Electron

Microscopic and Histomorphometric Analysis. *Clin. Oral. Implants Res.* **1998**, *9*, 195−207.
(32) Zhang, Y.; Chai, C.; Jiang, X. S.; Teoh, S. H.; Leong, K. W. Fibronectin Immobilized by Covalent Conjugation or Physical Adsorption Shows Different Bioactivity on Aminated-PET. *Mater. Sci. Eng., C* **2007**, *27*, 213−219.
(33) Salmerón-Sánchez, M.; Rico, P.; Moratal, D.; Lee, T. T.; Schwarzbauer, J. E.; García, A. J. Role of Material-Driven Fibronectin Fibrillogenesis in Cell Differentiation. *Biomaterials* **2011**, *32*, 2099−2105.
(34) Balguid, A.; Mol, A.; van Marion, M. H.; Bank, R. A.; Bouten, C. V. C.; Baaijens, F. P. T. Tailoring Fiber Diameter in Electrospun Poly(ε-caprolactone) Scaffolds for Optimal Cellular Infiltration in Cardiovascular Tissue Engineering. *Tissue Eng., Part A* **2009**, *15*, 437−444.